Controlled spatiotemporal excitation of metal nanoparticles with picosecond optical pulses

Tae-Woo Lee and Stephen K. Gray
Chemistry Division and Center for Nanoscale Materials, Argonne National Laboratory, Argonne, Illinois 60439, USA
(Received 8 June 2004; revised manuscript received 7 September 2004; published 28 January 2005)

We discuss realistic finite-difference time-domain simulations of chirped optical pulses interacting with silver nanowires and cone-shaped nanoparticles. These systems are differently shaped and larger than those previously studied [M. I. Stockman, S. V. Faleev, and D. J. Bergman, Phys. Rev. Lett. **88**, 067402 (2002)], but still allow for localized hot spots near the metal surfaces to be generated and controlled in a spatiotemporal manner. The control is made possible by chirping the pulses such that the effective frequency passes through surface plasmon resonances associated with different spatial regions of the nanostructure over the course of time. We demonstrate how this leads to counterintuitive, negative group velocities in some situations. The control is shown to scale with pulse duration from ≈150 fs to at least ≈2200 fs=2.2 ps, and we anticipate it to scale to longer durations. We further show that the response of such nanostructures to chirped pulses can provide a means of encoding or decoding optical signals, which could be verified experimentally.

DOI: 10.1103/PhysRevB.71.035423 PACS number(s): 78.67.−n, 73.20.Mf, 78.20.Bh

I. INTRODUCTION

The area of coherent control is about using coherent sources of excitation—e.g., lasers—in a variety of ingenious ways to achieve desired outcomes. Particular success in coherently controlling the spectroscopy and dynamics of atoms and molecules should be noted.[1–5] There is also great interest in the coherent excitation and control of a range of other systems, including, for example, semiconductors,[6] quantum dots,[7] biological systems,[8] and nanostructures.[9–17]

There is much current interest in the response of metal nanoparticles,[13–15] as well as near-field metallic probes or tips,[16,17] to ultrafast pulses. An interesting theoretical demonstration that one of the simpler tools of coherent control, a chirped femtosecond laser pulse, can be used to localize energy in nanostructures was given by Stockman, Faleev, and Bergman.[11] They showed how such pulses could concentrate energy at the apex of a hypothetical, thin V-shaped metallic nanostructure with dimensions much smaller than the applied wavelengths. As pointed out in Ref. 11, such small dimensions allow one to neglect electromagnetic retardation effects. Motivated in part by such results, we consider here a physical regime where the systems have dimensions comparable to operating wavelengths. We also investigate temporal behavior into the picosecond regime. Whereas Ref. 11 was primarily concerned with achieving extremely high intensities in localized regions, we focus on the detailed spatiotemporal behavior while the system interacts with the pulse, pointing out behavior that can be achieved. All these features will facilitate the experimental realization or practical application of coherent control phenomena in nanosystems.

We study the electrodynamics of metallic nanowires and cone-shaped metal nanoparticles interacting with chirped laser pulses ranging from femtosecond to picosecond durations. For the system dimensions considered here, one should use a rigorous computational approach that correctly includes, for example, retardation effects and a well-defined incident light pulse in terms of polarization and direction of propagation. Our calculations employ the finite-difference time-domain (FDTD) method,[18] which, when properly applied, leads to an accurate description of the wave propagation. Thus, the FDTD method is well suited to such time-domain problems. The FDTD method has recently been applied to several related problems.[19–22] We show how the properties of the chirped pulse can be used to control the spatiotemporal behavior of localized excitations or hot spots near the metal surfaces. We discuss how this is due to the creation of localized surface plasmon (SP) excitations[23] near the metal surface. Counterintuitively, apparent motion of hot spots in directions opposing the propagation direction of the incident light pulses can also be created with appropriate pulses. Such spatiotemporal control, while interesting from a fundamental point of view, could also have practical uses in the areas chemical sensors, optoelectronics, and communications. We show, for example, that the spatiotemporal behavior of surface plasmons in metal nanoparticles can be used to encode or decode digital information.

Section II below discusses the metallic nanostructures of interest to us (Sec. II A), the laser pulse properties (Sec. II B), and some details of the FDTD calculations (Sec. II C). Section III discusses our results on silver nanowires (Sec. III A), conelike silver nanoparticles (Sec. III B), and digital information encoding (Sec. III C). Section IV concludes.

II. COMPUTATIONAL DETAILS

A. Metal nanowire and nanoparticle systems

We consider certain metal nanowire and nanoparticle systems, each of which can be illustrated with the x-z plane diagram of Fig. 1. In the case of the nanowire, we imagine an infinitely long nanowire, surrounded by air, coming out of the plane of Fig. 1—i.e., invariance of the dielectric properties with respect to y. In this case, Fig. 1 displays the cross section of the nanowire in the x-z plane for any y value. The vertical or z dimension of the nanowire cross section is 250 nm, and its horizontal or x dimension varies linearly from 20 nm at its bottom to 140 nm at its top. The second system of interest is a conelike, cylindrically symmetric metal nanoparticle. In this case Fig. 1 depicts the x-z plane

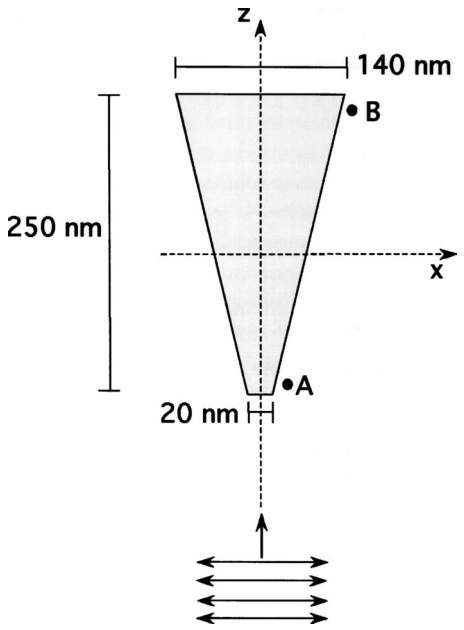

FIG. 1. Diagram of the nanowire and nanoparticle geometries considered. The grey area corresponds to silver. In the nanowire case, the nanowire is imagined to be infinitely extended along the *y* axis normal to the *x* and *z* axes. In the nanoparticle case, symmetry with respect to rotation about the *z* axis defines a conelike solid metal nanoparticle with a blunt lower nose. Points *A* and *B* near the bottom and top of the nanostructure are used in our analysis. Specifically, point *A* is 11.25 nm along *z* above the bottom of the nanowire and 2 nm along the *x* (or ρ) direction from the nanowire surface. Point *B* is 238.75 nm along *z* from the bottom of the nanowire and also 2 nm along the *x* direction away from the surface.

cross section for $y=0$ and the dielectric properties are taken to be invariant with respect to azimuthal rotation about the *z* axis. This produces a conelike particle with a flat bottom or nose. The nanoparticle is 250 nm high, and the diameter of its circular cross section in the *x*-*y* plane varies from 20 nm at its bottom to 140 nm at its top. This type of structure is also similar to a near-field scanning optical microscope (NSOM) tip.[16,17] In both cases we consider *x*-polarized light pulses moving vertically upward along *z*, as indicated.

When light interacts with metal nanoparticles it is possible for it to excite collective electronic resonances called surface plasmons.[23] SP's can arise if the real part of the metallic dielectric constant, for the applied wavelengths, takes on certain negative values. For silver nanosystems these wavelengths are typically in the 300–500 nm range. SP excitations are localized near metal surfaces with electric field intensities much higher than incident intensities. SP's are also relatively short lived with characteristic decay times less than 10 fs and are thus broad resonances spanning a range of incident wavelengths. Note that the SP excitations we will manipulate here can be best viewed as localized electromagnetic surface waves and not traveling waves or surface plasmon polaritons.[24] Nonetheless, through a careful choice of the incident pulse we will be able to create localized excitations that *appear* to move along the surfaces.

The character or field intensity pattern of an SP can vary with wavelength. It is well known that the peak SP resonance wavelength for metal spheres or cylinders tends to increase with nanoparticle size. We might therefore expect that the SP's for a given, less symmetrical structure, to vary in character with wavelength. For example, SP's localized mostly near the narrow, bottom portion of the nanostructure in Fig. 1 might have smaller wavelengths than those mostly localized near the wider, top portion. It is this simple expectation, which turns out to be true, that leads to our ability to obtain spatiotemporal control of intensity in such structures. In particular certain chirped pulses, designed to exhibit different effective frequencies (or wavelengths) at different times, can be expected to excite different spatial regions of the nanostructures at different times.

B. Chirped pulses

We consider incident pulses based on the form[25]

$$f(t) = A(t)\sin[\omega_0 t + \varphi(t)], \tag{1}$$

where $A(t)$ denotes a pulse envelope function, ω_0 is the carrier frequency, and a linear chirp is introduced by modulating the phase of the sinusoidal carrier function as follows:

$$\varphi(t) = \omega_0 \alpha t^2/\tau. \tag{2}$$

Inserting Eq. (2) into Eq. (1) and equating the argument of the sine function to $[\omega_{eff}(t)\ t]$ yields the effective frequency

$$\omega_{eff}(t) = \omega_0(1 + \alpha t/\tau). \tag{3}$$

The effective frequency changes linearly from $\omega_0(1-\alpha)$ to $\omega_0(1+\alpha)$ over the duration of the pulse which is taken to be from $t=-\tau$ to $+\tau$. A positive chirp—i.e., increasing effective frequency over the duration of the pulse—corresponds to $\alpha>0$ and a negative chirp—i.e., a decreasing effective frequency over the duration of the pulse—corresponds to $\alpha<0$. We use a standard Blackman-Harris window function[26] to define an envelope function $A(t)$ that smoothly changes from 0 to 1 to 0 as t varies from $=-\tau$ to 0 to $+\tau$.

Figure 2 illustrates the pulses produced by Eqs. (1) and (2). For this example we use $\omega_0=3.52$ eV ($\lambda_0=353$ nm), $\tau=15$ fs, and $|\alpha|=0.5$. Subpanels (a) and (b) represent the cases of negative ($\alpha<0$) and positive ($\alpha>0$) chirps, respectively. The rather small duration parameter τ and large magnitude chirp $|\alpha|$ were chosen to make the chirps easily evident in Fig. 2; more realistic pulses will be considered in our later calculations. It is interesting to note that the energy carried by each pulse is identical in terms of spectral content. Such opposite chirp pulses will be seen to lead to very different spatiotemporal behavior.

C. FDTD calculations

The finite-difference time-domain method involves simple spatial and temporal discretizations of the time-dependent form of Maxwell's equations and leads to relatively straightforward direct, time-stepping algorithms.[18] However, the description of metallic regions can be problematic if, as is the case for SP's, the complex, frequency-dependent nature of the dielectric constant is essential. (Even assuming the me-

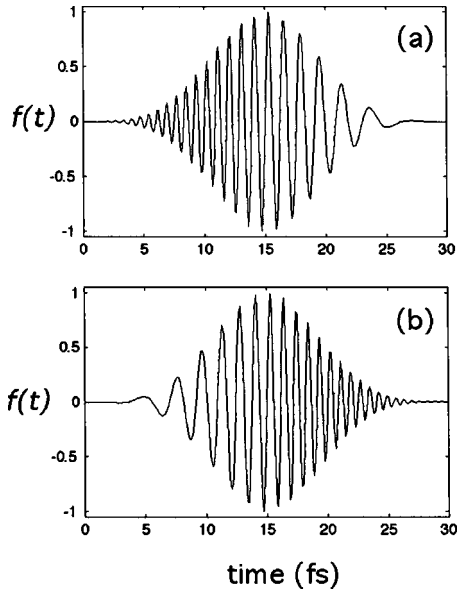

FIG. 2. Negative (a) and positive (b) frequency-chirped pulses. The pulses shown are somewhat shorter and more strongly chirped than the more experimentally achievable pulses that we employ in our detailed numerical work in order to show clearly the qualitative form of the chirped pulses.

tallic dielectric constant is real and frequency independent, the fact that it must be negative makes the simplest FDTD algorithm unstable.) However, the following time-dependent form of Maxwell's equations,[19]

$$\frac{\partial}{\partial t}\mathbf{E}(x,y,z,t) = \frac{1}{\varepsilon_{eff}(x,y,z)}[\nabla \times \mathbf{H}(x,y,z,t) - \mathbf{J}(x,y,z,t)],$$

$$\frac{\partial}{\partial t}\mathbf{H}(x,y,z,t) = -\frac{1}{\mu_0}\nabla \times \mathbf{E}(x,y,z,t),$$

$$\frac{\partial}{\partial t}\mathbf{J}(x,y,z,t) = a(x,y,z)\mathbf{J}(x,y,z,t) + b(x,y,z)\mathbf{E}(x,y,z,t), \tag{4}$$

can be solved in a stable manner with the FDTD method. In parts of space occupied by an ordinary dielectric material with a positive, real, and constant relative dielectric constant ε_R, $\varepsilon_{\text{eff}}=\varepsilon_R\varepsilon_0$ and $a=b=0$. In metallic parts of space, if one takes $\varepsilon_{\text{eff}}=\varepsilon_\infty\varepsilon_0$, $a=-\Gamma_p$, and $b=\varepsilon_0\omega_p^2$, then the solution of Eqs. (4) is equivalent to using a Drude form[23] for the complex, frequency-dependent metal's dielectric constant,

$$\varepsilon(\omega) = \varepsilon_\infty - \frac{\omega_p^2}{\omega^2 + i\Gamma_p\omega}. \tag{5}$$

Following Ref. 19 we use Drude parameters fit to empirical dielectric constant data for silver in a specific range of frequencies (or wavelengths). In particular we use $\varepsilon_\infty=8.296$, $\omega_p=11.585$ eV, and $\Gamma_p=0.203$ eV, appropriate for describing wavelengths in the range 300–500 nm (Ref. 19) or photon energies from 2.5 to 4 eV.

Some further comments on the Drude model discussed above and our optical pulses are in order. The interband transition region for bulk silver is near 4 eV (Ref. 27) and the Drude model used will be inappropriate for energies above 4 eV. The largest pulse bandwidth used in this study covers the "zero-to-zero" photon energy range from 3.0 eV to 4.0 eV; i.e., there is no spectral content outside this range. Assuming that the bulk silver dielectric constant is an appropriate description of our metal nanosystems, the Drude model employed here should therefore be adequate. For pulses with different spectral content, alternative Drude parametrizations and, if interband effects are important, the inclusion of Lorentzian terms [23] in the dielectric model might be required. The size of the nanosystem must also be considered. For example, a recent ultrafast time-resolved spectroscopy study showed that optical properties may deviate from bulk values for sufficiently small sizes.[27] For silver and gold, the study showed that this effect arises when the diameter of the particle becomes smaller than 10 nm. The smallest dimension used in our work is 20 nm.

The symmetry of the metal nanowire case results in a two-dimensional system similar in spirit to that studied in Ref. 19. With the axis system introduced in Fig. 1 we need only propagate E_x, E_z, and H_y field components, which in turn depend only on x, z, and t. The relevant FDTD equations are the same form as those in Ref. 19 except that in that reference the infinitely long nanowire axis was taken to be the z axis instead of the y axis used here. The computational domain is terminated by a uniaxial perfectly matched layer (UPML) (Ref. 18) to effectively absorb outgoing field components. The total-field–scattered field approach [18] was used to implement the initial chirped pulses, which are given by $E_z(x,z,t)=0$,

$$E_x(x,z_i,t) = A(t)\sin[\omega_{eff}(t)t - k_{eff}(t)z_i],$$

$$H_y(x,z_i,t) = (\varepsilon_0/\mu_0)^{1/2}A(t)\sin[\omega_{eff}(t)t - k_{eff}(t)z_i], \tag{6}$$

with $A(t)$ and $\omega_{eff}(t)$ as defined in Sec. II B and $k_{eff}(t)=\omega_{eff}(t)/c$. Note these pulses are injected into the system, over the initial time period $-\tau$ to τ defined by $A(t)$, along a given line in x at some fixed z value z_i, outside the nanowire, which also serves to separate the total and scattered fields. In practice, for the nanowire case, the computational domain consists of 600×1000 grid points in the x-z plane, with resolution is $\Delta x=\Delta z=0.5$ nm and time step $\Delta t=0.001\,07$ fs.

The three-dimensional (3D) conelike nanoparticle we also study is most efficiently modeled with a cylindrical coordinates (ρ,z,φ) FDTD algorithm.[18,28] In this approach, the six field components $(H_\rho,H_\varphi,H_z,E_\rho,E_\varphi,E_z)$ are expressed as general sine and cosine series in terms of φ. The x polarization of the initial condition (Fig. 1) allows one to focus only on the components E_ρ^c, E_z^c, and H_φ^c associated with $\cos(\varphi)$ and the components E_φ^s, H_ρ^s, and H_z^s associated with $\sin(\varphi)$ in such a series. Thus, while one must propagate six field components, computer time and memory are reduced in comparison with a Cartesian coordinates implementation because these components only depend on ρ and z. The initial pulse is

equivalent to the nanowire case one, i.e., it emanates out of the line $z=z_i$ for all x over the initial $t=-\tau$ to τ period, with $E_z^c=H_z^s=0$, and

$$E_\rho^c = E_x, \quad E_\varphi^s = -E_x,$$

$$H_\rho^s = H_y, \quad H_\varphi^c = -H_y, \tag{7}$$

with E_x and H_y given by Eq. (6). The computational domain in the nanoparticle case consists of 500×900 evenly spaced grid points in the ρ-z plane, which is comparable to $1000\times1000\times900$ points in a Cartesian coordinate system. As with the nanowire case, we use spatial resolution $\Delta\rho=\Delta z=0.5$ nm, UPML's are used to absorb outgoing field components, and the initial pulse was implemented with the total-field–scattered-field formulation.[18] Owing to a different stability limit,[28] the time step is slightly smaller, $\Delta t=0.000\,82$ fs.

The computational grids, time steps, and other details employed here were designed to yield time-domain intensities converged to better than 5%. We have verified this with convergence checks involving both smaller and larger grid sizes. Each calculation can require up to several hours computation time on a Pentium IV computer.

III. RESULTS

A. Nanowire systems

Motivation for determining the pulse parameters in Eqs. (1)–(3) is provided by carrying out preliminary calculations of the frequency response of the silver nanowire (Fig. 1) at positions *A* and *B*. Point *A* is close to the bottom of the nanowire cross section, and point *B* is close to the top of the nanowire cross section, as indicated in Fig. 1. The absolute square of the Fourier transforms of the electric field at positions *A* and *B*, given exposure to an arbitrary femtosecond pulse, shows SP resonance peaks near $\hbar\omega=3.7$ eV and 3.4 eV. The chirped pulses are then designed to exhibit effective frequencies spanning this range of frequencies over their durations.

We first consider the nanowire system exposed to chirped femtosecond pulses with $\tau=78.5$ fs, central carrier frequency $\hbar\omega_0=3.52$ eV, and $\alpha=-0.12$, 0, and 0.12. The full width at half maximum (FWHM) of such a pulse is 38.7 fs. Figure 3 shows the envelope of the electric field intensity ($|\mathbf{E}|^2$) observed as a function of time at two different locations, points *A* and *B*. The actual field oscillations are so frequent compared to the pulse durations that, for clarity here and from now on, we plot the intensity envelope which covers all the maxima.

Figures 3(a)–3(c) represent the cases of negative chirp ($\alpha=-0.12$), no chirp ($\alpha=0$), and positive chirp ($\alpha=0.12$), respectively. Since all cases use an identical pulse envelope, the *same* amount of total energy is carried in each pulse. Several features of the results are worth mentioning. First, controlling electromagnetic energy in a spatiotemporal manner on the subwavelength scale can indeed be achieved with the dynamic response of SP's. This is clearly evident with, for example, the negative chirp result showing region *A* being excited first, followed by *B* [Fig. 3(a)], the no chirp case having a more simultaneous excitation of both regions [Fig. 3(b)], and, interestingly, the positive chirp case showing *B* at the far end of the cross section of the nanowire gaining much more intensity than *A* at first [Fig. 3(c)]. This is consistent with the fact that the resonance frequency at region *A* is higher than that for region *B*, so that the time-varying carrier frequency of the negative chirp can pass through the resonance of the region *A* earlier than that of region *B*. In the positive chirp case, Fig. 3(c), the temporal SP excitations in regions *A* and *B* are reversed: the positive chirp passes through the resonance of the region *A* *later* than that of region *B*.

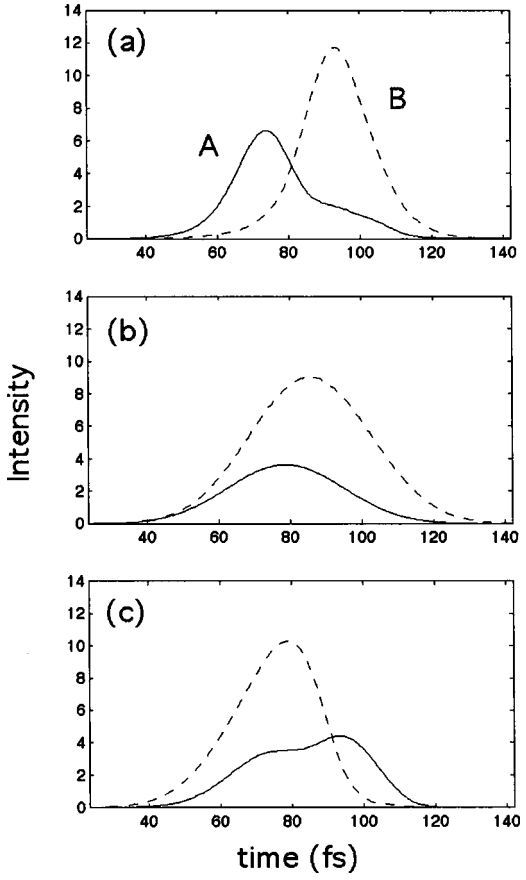

FIG. 3. Time-evolving intensity envelope at points *A* and *B* as the nanowire system in Fig. 1 interacts with the negative chirp (a) no chirp (b), and positive (c) chirp cases. The chirp magnitude is $|\alpha|=0.12$ and duration parameter $\tau=78.5$ fs.

We find the positive chirp case result of Fig. 3(c) interesting because the actual pulse emanates with positive group and phase velocity (along *z*) from a region below region *A* and thus overlaps region *A* first and then region *B*. However, the temporal progression of the localized spatial excitation is effectively from region *B* to region *A*, implying a negative (in *z*) group velocity. Detailed inspection of movies of the field intensity confirms a picture of positive phase velocity associated with the progression of individual maxima, but with the envelope of several maxima exhibiting a negative group velocity on average. While seemingly counterintuitive, the result is entirely consistent with how the positive chirp

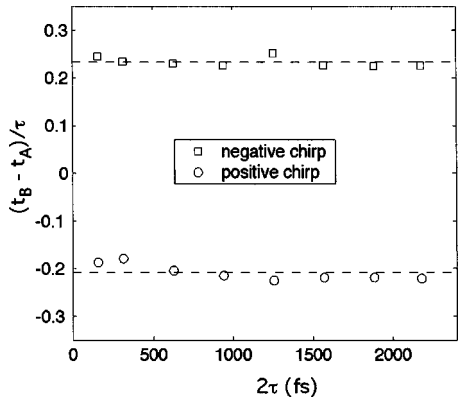

FIG. 4. Time separation of the peak intensity SP responses between regions *A* and *B*. The separations, t_B-t_A are normalized with pulse duration parameter τ and plotted as a function of full pulse duration 2τ.

has been defined; i.e., as time progresses the effective carrier frequency passes through SP resonances first associated with region *B* and then region *A*. The localized and damped nature of the SP excitations also plays a key role. We are not creating traveling surface plasmon polaritons (SPP's). Rather, we are sequentially exciting spatially localized SP resonances along the nanowire surface from the top to bottom in the case of Fig. 3(c). Each localized excitation decays in a 1–10 fs time scale, so that newer localized excitations, at more negative *z* stand out more and lead, on average, to a driven, negative flow of intensity from top to bottom. If we turn off the pulse at any given time, we do not find any significant continuation of the envelope of the excitation in a negative z direction, but rather behavior consistent with decay localized SP's.

The intensities shown in Fig. 3 are on a scale such that the maximum intensity of the incident pulse is unity. Intensity enhancements of about an order of magnitude are evident owing to the SP excitations. These enhancement levels are nonetheless smaller than what might be expected. (Somewhat larger intensity enhancements will occur for observation points closer to the metal surfaces.) The reason for this is the finite duration of the laser pulses and the fact that the frequency is never in resonance for very long. This is in contrast to the results of Ref. 11 which showed coherent excitations with much larger intensity enhancements. However, our nanostructures are different both in terms of shape and size than those of Ref. 11, and we also did not attempt to optimize our pulses in any way for intensity enhancement.

We conducted several nanowire simulations with longer pulse durations. The same parameters used as in the previous nanowire case (τ=78.5 fs) are chosen except pulse duration. The temporal delay of SP excitation between regions *A* and *B* is measured for each case. Figure 4 shows the peak-to-peak time delay normalized with a given pulse width, τ, as a function of full pulse duration 2τ. The results show that the time separations between the peaks associated with *A* and *B* increase linearly with pulse duration. In Fig. 5, the full time variation for the τ=628.3 fs case is presented. As with Fig. 3, just the envelopes of intensity maxima are displayed for clarity. By comparing Figs. 3 and 5 corresponding to ever longer

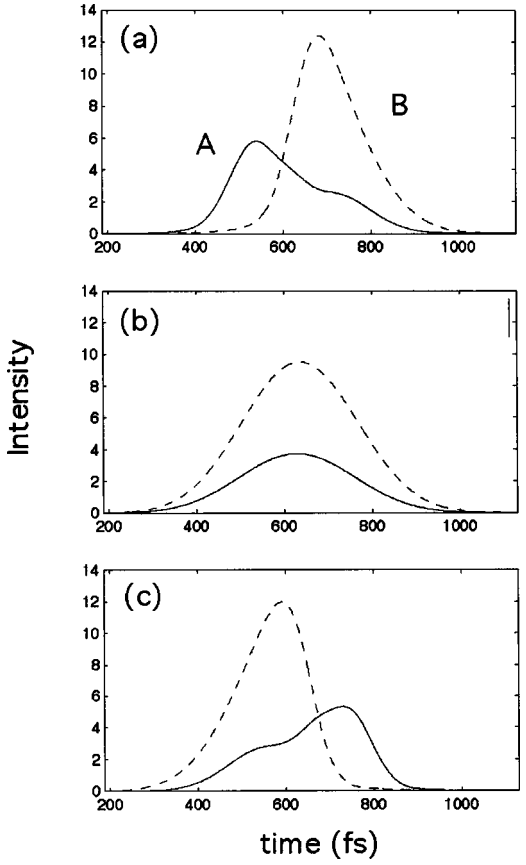

FIG. 5. Time-dependent intensity envelopes at points *A* and *B* in the nanowire system. Similar to Fig. 3 except that the pulse duration parameter is τ=628.3 fs.

pulse durations, it can be seen that the temporal variations of electric field intensity are very similar in shape for those cases. However, as indicated in Fig. 4, the temporal delay of the SP excitation between regions *A* and *B* becomes larger for longer pulses, while the unchirped case still remains as an almost simultaneous excitation. This implies the temporal scalability of the characteristics of SP excitation in such nanosystems. In other words, the longer pulse width, the more distinctive temporal discrimination of SP excitations in different spatial regions can be obtained. While, due to computational limitations, Fig. 4 extends to 2τ=2.2 ps, we anticipate that the results will scale to much longer times. We also conducted simulations for other chirp parameters than those displayed. The results show that the spatiotemporal discrimination becomes weaker as the absolute value of the chirp parameter decreases and, eventually, converges to the unchirped cases shown above.

The intensity responses of the system scale approximately with $t'=t/(2\tau)$. The time axes in Figs. 3 and 5 were all chosen to correspond to the same, scaled range t' =0.15–0.9 While only clear if one were to overlay the figures, the intensity variation becomes increasingly similar when viewed as a function of t' for increasing pulse length parameters τ.

B. Cone-shaped nanoparticles

As with the nanowire case above, two observation points *A* and *B* are set to compare the temporal variation of local

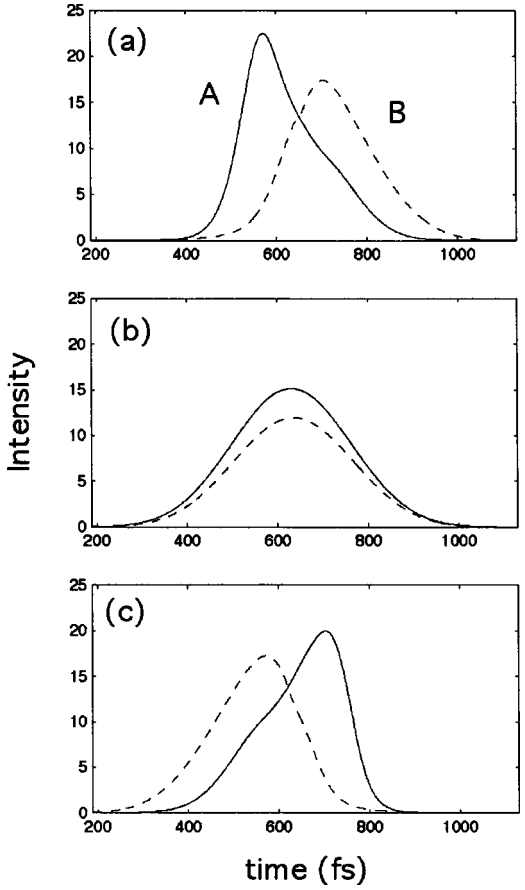

FIG. 6. Time-dependent intensity envelopes at points *A* and *B* as the cone-shaped nanoparticle system interacts with the negative chirp (a), no chirp (b), and positive chirp (c) cases with chirp magnitude $|\alpha|=0.12$ and duration parameter $\tau=628.3$ fs.

field intensities in two different locations near the nanoparticle (Fig. 1). If (x_A, z_A) denotes observation point *A* in the nanowire case above, then we use observation point $(\rho_A, z_A, \varphi_A)=(|x_A|, z_A, 0)$. We also carried out a preliminary frequency response analysis at points *A* and *B*, inferring the SP resonance frequencies near $\hbar\omega=3.55$ eV and 3.4 eV, similar to the nanowire case. We chose to study the central pulse frequency and width $\hbar\omega_0=3.47$ eV and $\tau=628.3$ fs, as well as chirps $\alpha=-0.12$, 0, and 0.12.

Figure 6 shows the intensity envelope variation in time for regions *A* and *B* for the three different chirp cases. The results are very similar to those obtained for the nanowire case with a similar pulse, Fig. 5. Thus, the negative chirp [Fig. 6(a)] leads to clear excitation of region *A* followed by region *B*, the no chirp case [Fig. 6(b)] has almost simultaneous excitation of the regions, and the positive chirp shows region *B* being excited prior to region *A*. We also conducted the FDTD simulations for different pulse widths. The results follow what we have seen in nanowire case. The spatiotemporal discrimination of the SP excitation is again almost linearly proportional to the width in time of the incident pulse, indicating good temporal scalability. The peak differences in time are 12.8 fs, 30.3 fs, and 131.5 fs for negative chirp and 14.0 fs, 30.0 fs, and 131.0 fs for positive chirp when incident pulse widths are $\tau=78.5$, 157.0, and 628.3 fs, respectively. Thus we have shown that there is nothing special about the more explicitly 2D nanowire configuration and that conelike 3D nanoparticles also display very similar spatiotemporal behavior.

C. Digital information from optical pulses

We have seen in the above two subsections that suitably chosen, chirped optical pulses can generate hot spots on certain metal nanosystems with controllable spatiotemporal behavior. An interesting twist on this is to use such spatiotemporal evolution to generate a new or more desirable signal than the originally applied one. Such manipulations could be of use in optoelectronics and communications.[25,29] In conventional optical data communication systems, for example, digitally formatted information is transferred along optical waveguides as pulsed optical signals. Since each pulse (or its absence) represents a digital signal of 1 (or 0) in a given clock cycle, it is essential to avoid overlap of adjacent pulses. This condition becomes one of the obstacles in using full capacity of the wide bandwidth of ultrashort pulses or chirped pulses. (Chirped pulses have larger bandwidth than unchirped pulses with same pulse duration.) In the chirped pulse case, the main factor limiting bit rate is not the bandwidth of the pulses but delay time for the sequence of pulses which must not overlap. This is also true for ultrashort pulses since chirped pulses can be considered as a result of ultrashort pulses spread out by group velocity dispersion. However, as we will demonstrate, nanosystems can decode the original digital information from severely overlapping pulses, suggesting a means of increasing the bit rate. Alternatively, one might wish to encode the digital information from the start with less obviously decodable overlapping pulses.

As a concrete example, imagine a digital system with a 150-fs clock cycle. A digital sequence (1,0,1) could be represented with an initial pulse spanning an approximate FWHM much less than 150 fs and another, similar pulse separated from the original by 300 fs. On the basis of intensities, over the first 150 fs one would read,"1," over the next 150 fs one would read "0," and over the final 150 fs one would read. "1." Suppose however the pulse sequence over the time period in question was given by Fig. 7(a), which corresponds to the envelope of the intensity maxima of two overlapping, negatively chirped pulses. Each chirped pulse has parameters $\alpha=-0.12$, $\omega_0=3.47$ eV, and $\tau=561$ fs (Sec. II B), with the duration parameter τ chosen such that when displaced by 300 fs in time there is significant overlap. The intensity envelope in Fig. 7(a) exhibits very-high-frequency oscillations in the middle time range owing to the superposition of different effective frequencies. Such high-frequency oscillations are not easily detected due to the finite response time of photodectors. A local time average of the intensity would be more representative of a measured signal. Figure 7(b) displays such a local time average based on a Gaussian window about each time point with $1/e$ full width of 20 fs. While Fig. 7(b) is now more consistent with the expected (1,0,1) string of digital information, the 0 corresponds to a very shallow minimum that might not be clearly discerned from 1 in practice.

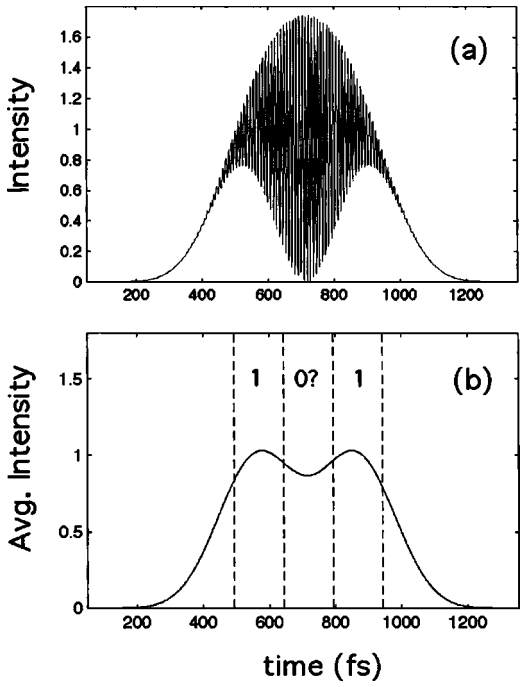

FIG. 7. (a) The time-dependent intensity envelope of a pulse sequence corresponding to two overlapping, chirped pulses. (b) The averaged intensity of the pulse sequence in (a).

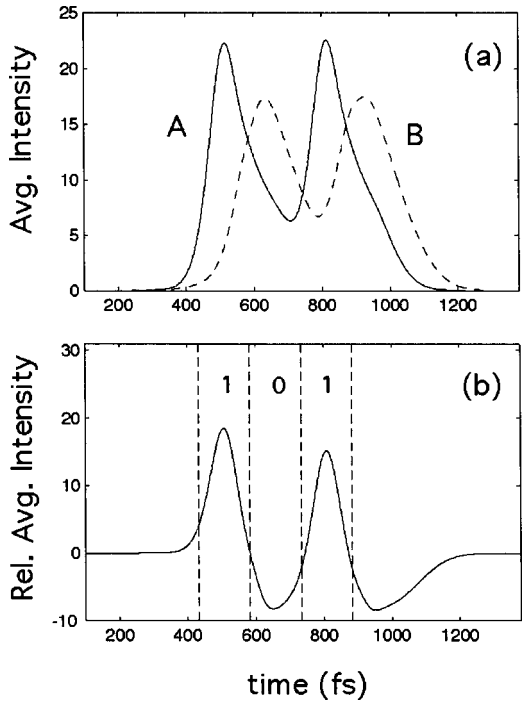

FIG. 8. (a) Averaged intensities for regions *A* and *B* of a cone-shaped silver nanoparticle exposed to the pulse of Fig. 7. (b) The difference of averaged intensities for *A* and *B*.

We now assume we are presented with the pulse sequence in Fig. 7 and wish to deduce an unambiguous digital signal. Suppose this pulse sequence is exposed to the 3D cone-shaped metal nanoparticle in the manner indicated by Fig. 1 and discussed in Sec. III B above. (We could equally discuss the nanowire case.) We carried out the corresponding FDTD calculations with the pulse sequence of Fig. 7 as source. During the simulation, we calculated the time-dependent intensities at regions *A* and *B* just as before. Figure 8(a) displays the resulting local time-averaged intensities. The intensity does not follow the incident pulse shape and the SP excitation in region *B* is delayed in time relative to region *A*. Since Fig. 8(a) shows the local time-averaged field intensities near regions *A* and *B*, it is also an approximate representation of an electric signal that could be obtained from the detection of SP's using, e.g., photodiodes designed to register fields near the corresponding regions. Once the optical signals are converted to electric signals (voltages), the signal from *B* can be *subtracted* from the *A* signal. Figure 8(b) shows the resulting difference signal. We define a 1 to be, within the given clock cycle, a predominantly positive-valued difference signal with a pronounced maximum. A 0 is defined to be a predominantly negative-valued signal. With these definitions, Fig. 8(b) readily yields the correct (1,0,1) digital sequence. Note also that the delay time between maxima of the difference signal is 300 fs, which now agrees well with original pulse delay time. Thus, for a given digital clock cycle, the nanoparticle system successfully decodes severely overlapping optical signals.

If one were to feed the nanoparticle system a well separated sequence of pulses, a pattern of maxima consistent with the original signal will result upon subtraction of signal *B* from signal *A*. One can infer from Fig. 6(a), for example, that the difference signal for an isolated pulse would have just one positive-valued maximum over its cycle—i.e., would be interpreted to be a 1 as it should be. Thus the nanoparticle system will still produce the correct result if the pulses are not overlapping.

IV. CONCLUDING REMARKS

In this paper we studied, with a realistic time-domain computational electrodynamics approach, how hot spots near the surfaces of certain metal nanowires and nanoparticles could be generated with chirped optical pulses. Remarkable spatiotemporal control could be achieved, including counter-intuitive motion of hot spots against the light propagation direction. This control was made possible by designing the chirp such that the effective frequency of the pulse resonates with different SP excitations located along the nanostructure over the duration of the pulse. Along with the pioneering theoretical demonstration of Stockman, Faleev, and Bergman[11] that localized coherent excitation of small metallic nanostructures is possible, we hope that such results will stimulate new theoretical and experimental explorations of such possibilities.

Our calculations involved specific system dimensions and shapes (see Sec. II A and Fig. 1). It is of course possible to achieve control with other dimensions and shapes. For example, simply increasing the height of the nanowire cross section or cone height (Fig. 1) beyond 250 nm has little effect on the time-domain results as long as the *x* dimensions at top and bottom are kept fixed. This is because the effective SP resonance frequencies near bottom (*A*) and top (*B*) are

essentially the same. For example, we have obtained similar results with cone-shaped nanoparticles of height 500 nm. Decreasing the height, within reason, should also have little effect, although the adiabatic variation of the SP resonance may come into question at some shorter heights. Regarding system widths, of course, the SP frequency tends to decrease with increasing width or x dimension in Fig. 1. Therefore one can choose widths appropriate to some prespecified spectral range for the chirp. The shape can also be varied; i.e., the specific conelike shape of Fig. 1 is not necessary. The particle shape should be such that its width, for some heights, is sufficiently different to permit different effective SP resonance frequencies that can be spanned by the chirp.

We also discussed how the response of such nanosystems to chirped pulses could be used to encode or decode digital information. In particular, it was proposed in Sec. III C, based on rigorous simulations, that two overlapping chirped pulses could be clearly distinguished by a cone-shaped metal nanoparticle. It is also possible that such ideas could be of relevance to chemical sensing. For example, one can imagine applying a chirped pulse such that one knows certain regions of the nanoparticle, at certain times, are excited. The spectral response of molecules near such hot spots should be enhanced (e.g., surface-enhanced Raman spectroscopy[30,31]). Applying various time-delayed probe pulses could then lead to transient spectral responses indicative of whether or not molecules are near a given place on the nanoparticle.

The spatiotemporal behavior studied here, including, for example, the signal encoding and decoding discussed in Sec. III C and above, can be observed experimentally. One must consider both how to infer the optical intensity near specific nanoparticle regions and how to time resolve this information. Regarding spatial resolution and considering the nanosystems with dimensions indicated in Fig. 1, the detection of field intensities near regions A and B can be performed with microscopy using a high-numerical-aperture microscope objective. In this scenario, local scatterers, such as defects or small particles, are placed in region A or B. This microscopy can then map out the field intensity in two different regions. If one needs more localized information, near-field scanning optical microscopy[16,17] could be used. In this scenario, field intensity will be detected by positioning the probe near region A or B. The time resolution of such information can also be determined as follows. Noting that the temporal behavior of SP's is scalable in time for a given pulse duration, the most simple approach is to use a p-i-n-type photodetector[25] with a slightly longer duration ($>$10 ps) chirped pulse than those explicitly considered here. The response time of the photodiode is then fast enough to time resolve the signals. The response to ultrashort pulses could also be experimentally observable, if one uses ultrafast cross-correlation techniques.

The analysis presented here was based on realistic simulations of single chirped pulses and two overlapping chirped pulses interacting with metal nanostructures. Pulse trains may also be of interest. However, if a train of femtosecond pulses with MHz repetition rate is considered, for example, it is evident that each pulse can be treated as a separate event because the SP response will have damped out by the time the next pulse hits. Obviously, the situation changes for much more closely spaced pulse sequences or more general pulse shapes.

ACKNOWLEDGMENTS

We thank Gary Wiederrecht for many helpful discussions. This work was supported by the U.S. Department of Energy, Office of Basic Energy Sciences, Division of Chemical Sciences, Geosciences, and Biosciences under DOE Contract No. W-31-109-ENG-38.

[1] D. J. Tannor and S. A. Rice, Adv. Chem. Phys. **70**, 441 (1988).
[2] P. Brumer and M. Shapiro, Annu. Rev. Phys. Chem. **43**, 257 (1988).
[3] W. S. Warren, H. Rabitz, and M. Dahleh, Science **259**, 1581 (1993).
[4] H. Kawashima, M. M. Wefers, and K. A. Nelson, Annu. Rev. Phys. Chem. **46**, 627 (1995).
[5] T. Brixner, N. H. Damrauer, and G. Gerber, in *Advances in Atomic, Molecular, and Optical Physics*, edited by B. Bederson and H. Walther, (Academic Press, San Diego, 2001), Vol. 46, pp. 1–54.
[6] J. Erland, V. G. Lyssenko, and J. M. Hvam, Phys. Rev. B **63**, 155317 (2001).
[7] X. Q. Li, Y. W. Wu, D. Gammon, T. H. Stievater, D. S. Katzer, D. Park, C. Piermarocchi, and L. J. Sham, Science **301**, 809 (2003).
[8] J. L. Herek, W. Wohlleben, R. J. Cogdell, D. Zeidler, and M. Motzkus, Nature (London) **417**, 533 (2002).
[9] J. H. Hodak, A. Henglein, and G. V. Hartland, J. Phys. Chem. B **104**, 9954 (2000).
[10] M. I. Stockman, Phys. Rev. Lett. **84**, 1011 (2000).
[11] M. I. Stockman, S. V. Faleev, and D. J. Bergman, Phys. Rev. Lett. **88**, 067402 (2002).
[12] K. Komori, G. Hayes, T. Okada, B. Deveaud, X. L. Wang, M. Ogura, and M. Watanabe, Jpn. J. Appl. Phys., Part 1 **41**, 2660 (2002).
[13] S. Link and M. El-Sayed, Annu. Rev. Phys. Chem. **54**, 331 (2003).
[14] J. Lehmann, M. Merschdorf, W. Pfeiffer, A. Thon, S. Voll, and G. Gerber, Phys. Rev. Lett. **85**, 2921 (2000).
[15] J. H. Hodak, A. Henglein, and G. V. Hartland, J. Phys. Chem. B **104**, 9954 (2000).
[16] E. J. Sanchez, L. Novotny, and X. S. Xie, Phys. Rev. Lett. **82**, 4014 (1999).
[17] A. Pack, M. Hietschold, and R. Wannemacher, Ultramicroscopy **92**, 251 (2002).
[18] A. Taflove and S. C. Hagness, *Computational Electrodynamics: The Finite-Difference Time-Domain Method*, 2nd ed. (Artech House, Boston, 2000).
[19] S. K. Gray and T. Kupka, Phys. Rev. B **68**, 045415 (2003).
[20] J. M. Oliva and S. K. Gray, Chem. Phys. Lett. **379**, 325 (2003).

[21] G. A. Wurtz, J. S. Im, S. K. Gray, and G. P. Wiederrecht, J. Phys. Chem. B **107**, 14191 (2003).
[22] L. Yin, V. K. Vlasko-Vlasov, A. Rydh, J. Pearson, U. Welp, S.-H. Chang, S. K. Gray, G. C. Schatz, D. E. Brown, and C. W. Kimball, Appl. Phys. Lett. **85**, 467 (2004).
[23] C. F. Bohren and D. R. Huffman, *Absorption and Scattering of Light by Small Particles* (Wiley, New York, 1983).
[24] A. V. Zayats and I. I. Smolyaninov, J. Opt. A, Pure Appl. Opt. **5**, S16 (2003).
[25] A. Yariv, *Optical Electronics in Modern Communications*, 5th ed. (Oxford University Press, New York, 1997).
[26] A. H. Nuttall, IEEE Trans. Acoust., Speech, Signal Process. **29**, 84 (1981).
[27] C. Voisin, D. Christofilos, P. A. Loukakis, N. Del. Fatti, F. Vallée, J. Lermé, M. Gaudry, E. Cottancin, M. Pellarin, and M. Broyer, Phys. Rev. B **69**, 195416 (2004).
[28] D. W. Prather and S. Shi, J. Opt. Soc. Am. A **16**, 1131 (1999). N.b. it appears that there are some typographical errors in Eqs. (4)–(10).
[29] A. Rogers, *Essentials of Optoelectronics with Applications* (Chapman and Hall, New York, 1997).
[30] A. Wokaun, Mol. Phys. **56**, 1 (1985).
[31] S. Nie and S. R. Emory, Science **275**, 1102 (1997).